HHS Public Access

Author manuscript

Nature. Author manuscript; available in PMC 2015 June 04.

Published in final edited form as:

Nature. 2014 December 4; 516(7529): 108–111. doi:10.1038/nature13949.

Transcriptional regulation of autophagy by an FXR/CREB axis

Sunmi Seok[1,#], **Ting Fu**[1,#], **Sung-E Choi**[1,2], **Yang Li**[3], **Rong Zhu**[4], **Subodh Kumar**[1], **Xiaoxiao Sun**[4], **Gyesoon Yoon**[2], **Yup Kang**[2], **Wenxuan Zhong**[4], **Jian Ma**[3], **Byron Kemper**[1], and **Jongsook Kim Kemper**[1,*]

[1]Department of Molecular and Integrative Physiology, University of Illinois at Urbana-Champaign, Urbana, IL 61801, USA

[2]Institute for Medical Science, Ajou University School of Medicine, Suwon 442-749, Republic of Korea

[3]Department of Bioengineering and the Institute for Genomic Biology, University of Illinois at Urbana-Champaign, Urbana, IL 61801, USA

[4]Department of Statistics, University of Georgia, Athens, GA 30602, USA

Abstract

Lysosomal degradation of cytoplasmic components by autophagy is essential for cellular survival and homeostasis under nutrient-deprived conditions[1–4]. Acute regulation of autophagy by nutrient-sensing kinases is well defined[3, 5–7], but longer-term transcriptional regulation is relatively unknown. Here we show that the fed-state sensing nuclear receptor FXR[8, 9] and the fasting transcriptional activator CREB[10, 11] coordinately regulate the hepatic autophagy gene network. Pharmacological activation of FXR repressed many autophagy genes and inhibited autophagy even in fasted mice and feeding-mediated inhibition of macroautophagy was attenuated in FXR-knockout mice. From mouse liver ChIP-seq data[12–15], FXR and CREB binding peaks were detected at 178 and 112, respectively, of 230 autophagy-related genes, and 78 genes showed shared binding, mostly in their promoter regions. CREB promoted lipophagy, autophagic degradation of lipids[16], under nutrient-deprived conditions, and FXR inhibited this response. Mechanistically, CREB upregulated autophagy genes, including *Atg7, Ulk1, and Tfeb*, by recruiting the coactivator CRTC2. After feeding or pharmacological activation, FXR trans-repressed these genes by disrupting the functional CREB/CRTC2 complex. This study identifies the novel FXR/CREB axis as a key physiological switch regulating autophagy, resulting in sustained nutrient regulation of autophagy during feeding/fasting cycles.

Correspondence and material request should be addressed to J. Kim Kemper, jongsook@illinois.edu.
[#]SS and TF equally contributed to this study.

Author contribution

SS, TF, and JK designed research; SS, TF, SC, and SK performed experiments; SS, TF, SC, SK, GY, YK, BK, and JK analyzed data; YL, RZ, XS, WZ, and JM analyzed ChIP-seq genomic data, and SS, TF, BK, and JK wrote the paper.

The authors declare no conflict of interest.

Metabolic nuclear receptors function as intracellular biosensors for lipid metabolites and nutrients, including bile acids and fatty acids, and transduce the nutrient signals into transcriptional programming to maintain homeostasis[8, 9]. The nuclear receptor FXR is activated by elevated bile acid levels after feeding and controls postprandial metabolic responses[8, 9]. Since FXR is a fed-state sensing gene regulator, we postulated that FXR transcriptionally represses hepatic autophagy in the postprandial period.

From mouse liver ChIP-seq data[12, 13], FXR binding peaks were detected near transcription start sites (TSS) of 178 of 230 autophagy-related genes involved in key autophagic processes (Supplementary Table 1, selected genes displayed in Extended Data Fig. 1a). FXR, therefore, may directly repress hepatic autophagy. To confirm the ChIP-seq results, liver ChIP analysis was performed in mice treated with GW4064, a specific agonist of FXR, rather than bile acids which activate multiple signaling pathways[9]. Treatment with GW4064 in fasted mice increased FXR occupancy at many autophagy genes and decreased mRNA levels of most of these genes in WT mice, but not in FXR-knockout (KO) mice, and also decreased their pre-mRNA levels (Fig. 1a, b, Extended Data Fig. 1b–d). Activation of FXR, thus, increased its occupancy at many autophagy genes and repressed their expression.

We next tested whether activation of FXR suppresses macroautophagy. Fasting increased the number of autophagic vesicles in liver, but the increase was significantly blunted by GW4064 treatment (Fig. 1c). Mitochondria in double membrane autophagosomes or autolysosomes, known as mitophagy, were detected in fasted WT mice but not after GW4064 treatment. Increased abundance of LC3-II, LC3 conjugated with phosphatidylethanolamine, is an indicator of autophagic flux[17] while the autophagosome adaptor p62/SQSTM1 accumulates when autophagy is inhibited[17]. Treatment with GW4064 decreased LC3-II and increased p62 levels in mouse liver extracts (Fig. 1d), and decreased LC3-II levels were observed in hepatocytes after lysosomal inhibition with bafilomycin A1 (Fig. 1e) or chloroquine (Extended Data Fig. 2a). These results indicate that FXR inhibits autophagy by transcriptionally repressing autophagy components, likely independent of lysosomal function.

To avoid confounding in vivo effects, such as induction of intestinal FGF19 by FXR[18], direct FXR effects on autophagy were examined in Hepa1c1c7 cells. The increase in GFP-LC3 puncta in cells incubated in HBSS starvation media, was attenuated by GW4064 treatment, but not if FXR was also downregulated (Fig. 1f). These findings indicate that FXR directly inhibits autophagy.

Since FXR is activated after feeding by bile acids, we tested whether FXR regulates autophagy under physiological conditions. The decrease in GFP-LC3 puncta after feeding in WT mice was markedly attenuated in FXR-KO mice (Fig. 2a, Extended Data Fig. 2b) and feeding decreased LC3-II levels and increased p62 levels in WT, but not in FXR-KO, mice (Fig. 2b). These findings indicate that FXR acts as a key physiological repressor of autophagy in the fed-state.

After feeding, autophagy components are suppressed by the nutrient-sensing mTOR/S6 kinase pathway[3, 5–7], which potentially could mediate FXR inhibition of autophagy.

Activation or downregulation of FXR resulted in expected changes in LC3-II levels, but no changes in phosphorylated S6 (p-S6) levels (Fig. 2c). Similar effects were observed after GW4064 treatment in hepatocytes (Fig. 2d) and in liver extracts (Fig. 2e). Further, treatment with rapamycin, an inhibitor of mTOR, increased LC3-II levels as expected, and co-treatment with GW4064 prevented the increase without changing the p-S6 levels (Fig. 2f). These results, suggest that FXR-mediated inhibition of autophagy appears to be independent of mTOR activation.

To further examine how FXR inhibits autophagy genes, we analyzed DNA binding motifs in FXR binding peak regions detected by ChIP-seq[12]. IR1 DNA binding motifs for FXR were not detected in sequences common to the FXR peak regions, but binding sites for several transcription factors (Supplementary Table 2) were detected including the top scoring motifs, TGACGT(C/T)(A/T), for CREB (Fig. 3a), a key transcriptional activator that drives fasting responses[10, 11]. Remarkably, in published liver ChIP-seq data for CREB[15, 19] and FXR[12, 13], CREB peaks were detected at 112 of 230 autophagy genes (Supplementary Table 3) and overlapped with FXR peaks in 78 genes (Fig. 3b, Supplementary Table 4) mostly within 1 kb of the TSS (Supplementary Table 3). Selected autophagy-related genes with overlapping FXR and CREB binding sites are listed in Fig. 3c and peaks are displayed in Extended Data Fig. 3a. Co-occupancy of FXR and CREB at these genes was confirmed in re-ChIP assays (Extended Data Fig. 3b). Downregulation of CREB decreased expression of autophagy genes (Fig. 3d) and reduced the number of LC3-II GFP puncta (Fig. 3e) in hepatic cells. These results suggest that CREB is a novel transcriptional activator of autophagy and that FXR may antagonize the CREB activity.

We next examined autophagic degradation of lipids, known as lipophagy[16]. Lipophagy, detected by co-staining of LC3 puncta with BODIPY, in fasted cells was reduced by downregulation of CREB (Fig. 3f). Further, overexpression of CREB reversed the inhibition of autophagy mediated by downregulation of Atg7 (Extended Data Fig. 4a, b). In contrast, downregulation of FXR increased lipophagy in non-fasted cells (Fig. 3g) and activation of FXR decreased lipophagy in fasted cells (Extended Data Fig. 4c). These results suggest that CREB and FXR oppositely regulate lipophagy in response to nutritional conditions.

To examine regulation of autophagy genes by FXR and CREB, an *Atg7 or Tfeb* DNA fragment that contained FXR and CREB binding peaks was inserted into a luciferase vector. Overexpression of CREB and its coactivator CRTC2[10] increased while overexpression of FXR inhibited luciferase activity (Fig. 4a). Mutation of the CREB site or downregulation of CREB blocked the FXR inhibition (Extended Data Fig. 5a, b). *Tfeb-luc* activity that was increased by CREB/CRTC2 was attenuated by FXR, but not by other nuclear receptors (Extended Data Fig. 5c). In CoIP studies, CREB interaction with CRTC2 was blocked while interaction with FXR was increased by GW4064 treatment (Extended Data Fig. 5d). In GST-pull down studies, CREB interacted with the C-terminal domain of FXR (Extended Data Fig. 5e). These results suggest that FXR may trans-repress autophagy genes by directly interacting with CREB and suppressing its activity. Supporting this conclusion, a DNA binding-deficient FXR mutant did not activate *FXRE-luc* activity but repressed *Tfeb-luc* activity (Extended Data Fig. 5f, g).

The functional interaction of FXR and CREB/CRTC2 was next examined by ChIP assay. Occupancy of CREB at autophagy genes was not changed, while that of FXR and CRTC2 was increased and decreased, respectively, and RXRα occupancy was barely detectable after GW4046 treatment (Extended Data Fig. 6a, b). In re-ChIP assays, GW4064 treatment decreased CRTC2 and increased FXR occupancies at CREB-bound autophagy genes, including *Atg7, Tfeb, and Ulk1* in WT mice, but not in FXR-KO mice (Fig. 4b, Extended Data Fig. 6c, d). Downregulation of CREB decreased FXR occupancy, suggesting that CREB is important for FXR recruitment (Extended Data Fig. 6e) and similar effects were observed in mice fed cholic acid chow (Extended Data Fig. 7a, b). In gel shift assays with an *Atg7* probe, FXR and CRTC2 individually formed complexes with CREB, and FXR caused dissociation of the CREB/CRTC2 complex and formation of a CREB/FXR complex (Fig. 4c). Similar results were observed with *Tfeb or Ulk1* probes (Extended Data Fig. 6f–h). Remarkably, activation of FXR was required for the FXR competition (Fig. 4d). Occupancy of FXR at the *Atg7, Ulk1, and Tfeb* genes correlated with increased repressing and decreased activating histone marks and increased occupancy of the corepressors, NcoR and SMRT (Fig. 4e, Extended Data Fig. 7c, d), suggesting formation of a repressive transcriptional complex. These results indicate that FXR trans-repressed autophagy genes by disrupting the CREB/CRTC2 complex.

We next examined whether physiological activation of FXR upon feeding dissociates CRTC2 from the CREB complex. Consistent with previous studies[10], CRTC2 was present in the nucleus in fasted animals and largely excluded from the nucleus in fed WT, but not FXR-KO, mice (Fig. 4f, Extended Data Fig. 8a). In contrast, nuclear localization of FXR was markedly increased by feeding or GW4064 treatment, while FXR was detected in both nucleus and cytoplasm during fasting (Extended Data Fig. 8b, c). Fasting increases CREB and CRTC2 activity by phosphorylation and dephosphorylation, respectively[10]. p-CREB was detected in the nucleus in fasted mice, whereas p-CRTC2 (S171) and CRTC2 were in the cytoplasm of fed mice, but the feeding-induced cytoplasmic localization of p-CRTC2 (S171) and CRTC2 was partially reversed in FXR-KO mice (Fig. 4g, Extended Data Fig. 8a). Fasting increased p-PKA levels, whereas p-PKB was undetectable and p-AMPK was not changed (Extended Data Fig. 8d, e). GW4064 inhibition of *Atg7 and Tfeb genes* was attenuated by expression of a p-defective CRTC2-S171A mutant constitutively retained in the nucleus[10] but overexpression of FXR reversed this effect (Extended Data Fig. 8f–h). These data suggest that both the phosphorylation status of CREB/CRTC2 and disruption of the CREB/CRTC2 complex by activated FXR are likely important for CREB-dependent fed-state regulation of autophagy genes.

In re-ChIP assays, feeding substantially increased FXR occupancy at CREB-bound genes, while occupancy of CRTC2 was decreased (Fig. 4h, i, Extended Data Fig. 9a, b). In contrast, in FXR-KO mice, the feeding-mediated decrease was reversed, but only partially. Reductions in the mRNA and pre-mRNA levels of these genes after feeding were partially or fully blocked in FXR-KO mice (Extended Data Fig. 9c, d). These partial effects in FXR-KO mice suggest that other meal-related signals also contribute to autophagy gene regulation. Indeed, treatment with insulin, FGF19, or GW4064 downregulated autophagy genes to different extents, in a gene-specific manner (Extended Data Fig. 9e). These findings

reveal that disruption of the CREB/CRTC2 complex and trans-repression of autophagy genes by activated FXR is one mechanism by which autophagy is inhibited after feeding.

The present study identifies FXR and CREB as novel transcriptional regulators of the autophagy gene network (Fig. 4j). During nutrient-deprived fasting, CREB/CRTC2 activate transcription of autophagy-related genes involved in multiple autophagic processes. Upon feeding, bile-acid-activated FXR (mimicked by GW4064) interacts with CREB, disrupts the CREB/CRTC2 complex, resulting in decreased nuclear CRTC2 levels, formation of a repressive transcriptional complex, and inhibition of autophagy genes. In addition, feeding-induced changes in phosphorylation of CREB and CRTC2 are also important disrupting the CREB/CRTC2 complex. The hepatic FXR/CREB axis may also be relevant to other tissues since FXR and CREB are expressed in many tissues. Further, the CREB/CRTC2 complex also activates transcription programs of gluconeogenesis and ER stress[10, 11]. It will be interesting to see whether FXR more generally inhibits CREB-activated genes.

Remarkably, both FXR and CREB regulate expression of TFEB, a key activator of autophagy/lysosomal genes[20, 21]. Notably, some autophagy genes appear to be regulated predominantly either by CREB or TFEB or by both (Extended Data Fig. 4d, e and Supplemental Table 5). In addition, other nutrient-sensing regulators, such as PPARα (accompanying manuscript), likely transcriptionally regulate autophagy. Only about 45% of FXR target autophagy genes had shared FXR/CREB binding so that FXR may act by multiple mechanisms that are gene- or DNA context-specific. FXR may trans-repress by disrupting the CREB/CRTC2 complex or by competing with PPARα for DNA binding, or both mechanisms may occur in the same gene. PKA-activated CREB may also be important early in fasting and dominant after feeding following a short fast and fatty acid-activated PPARα may be more important after prolonged fasting followed by refeeding. Supporting this idea, time-dependent occupancy of CREB/CRTC2 and PPARα/PGC-1α after fasting was observed at different regions of *Atg7 and Lc3a* genes (Extended Data Fig.10).

Autophagy is known to be crucial for cellular survival under extremely stressful conditions, but the present study demonstrates that it occurs physiologically during fasting/feeding cycles by regulation of FXR and CREB and also mediates lipid catabolic functions. Nutrient-sensing kinases, including mTOR, rapidly decrease activity and/or stability of core autophagic proteins. In contrast, transcriptional regulation by FXR and CREB, which is likely independent of the acutely acting mTOR, is slower and more persistent, which should effectively sustain regulation of autophagy for longer period of times.

Defective autophagy has been implicated in many human diseases but excess autophagy promotes cell death and also tumor progression[3, 22, 23]. In this regard, the nutrient-sensing FXR/CREB axis that tightly regulates the autophagy gene network may present new molecular targets for treating diseases associated with autophagy dysfunction, including metabolic disorders, neurodegenerative disease, and cancer.

Methods

Reagents

Antibodies were purchased for FXR (sc-13063), CREB (sc-186), CRTC2 (sc-46272, sc-271912), RNA pol II (sc-9001), NcoR (sc-8994), SMRT (sc-1612), p300 (sc-584), PGC-1α (sc-13067), H3K27-me2 (Abcam 050851), H3K4-me2 (Abcam 8580), ubiquitin (sc-9133), lamin A (sc-20680), β-tubulin (sc-5274), and actin (sc-1616) from Santa Cruz Biotechnology; for p(S133)-CREB (#9198S), LC3 (#4108), p62 (#5114), S6 kinase (#9202), p-S6 kinase (#9208), and ATG7 (#2631) from Cell Signaling; and for p(S171)-CRTC2 (bs-3415R) from Bioss USA. Mouse CREB siRNA was purchased from Thermo Scientific, FXR siRNA and control siRNA from Dharmacon, and Atg7 siRNA from Life Technologies (AM16708).

In vivo experiments

Eight to twelve week old male C57BL/6 mice and FXR-KO mice were used for in vivo animal studies. Mice were fasted for 10 h and treated with vehicle or GW4064 (30 mg/kg, i.p.) for 6 h, or were fasted or refed for 6 h. For EM studies, liver samples were stained with uranyl acetate/lead citrate and then imaged by TEM (EM902A; Carl Zeiss). For FXR activation assays, 10–12 week old male C57BL/6J mice or FXR-KO (Jackson lab) were fasted for 10 h and then injected i.p. with GW4064 (30 mg/kg) for 6 h or fed normal chow or 0.5% cholic acid (CA)-supplemented chow for 6 h. Then, livers were collected for molecular, biochemical, and imaging analyses. Adenoviral experiments were performed as previously described[24–26]. Ad-GFP-LC3 ($0.5–1\times10^9$ active particles/mouse in 200 μl PBS) was injected via tail vein into WT or FXR-KO mice, and 1 week later, the mice were fasted overnight and livers were collected. The frozen or paraffin-embedded liver sections were prepared for staining. In vivo experiments were approved by the Institutional Animal Care and Use and Biosafety Committees.

Liver transmission electron microscopy

Mouse liver was fixed using Karnovsky's fixative solution [1% paraformaldehyde, 2% glutaraldehyde, 2 mM $CaCl_2$, and 100 mM sodium cacodylate (pH 7.4)] for 2 h and washed with 100 mM sodium cacodylate (pH 7.4). After post-fixing with 1% osmium tetroxide and 1.5% potassium ferrocyanide for 1 h, mice livers were dehydrated with 50–100% alcohol and stained en bloc with 0.5% uranyl acetate. The liver tissues were embedded in Poly/Bed 812 resin (Pelco), polymerized, and sectioned using a Reichert Jung Ultracut S microtome (Leica, Wetzetlar) and stained with uranyl acetate and lead citrate. The liver tissue was imaged by transmission electron microscopy (EM902A; Carl Zeiss).

Histology and immunohistochemistry

For in vivo detection of hepatic autophagy, frozen or paraffin-embedded samples of liver expressing GFP-LC3 via adenoviral infection were fixed with 4% paraformaldehyde and nuclei were stained with DAPI and images were taken by confocal microscopy and analyzed by ZEN software (Zeiss LSM700). GFP-LC3 puncta were counted in 30 cells for each group and the average number per cell is reported. For monitoring endogenous FXR and CRTC2

localization, paraffin-embedded liver slides were incubated with their primary antibody for 2 h and with secondary antibody, Alexa 647 goat anti-mouse or anti-rabbit IgG for 1 h. Nuclei were labeled with DAPI and images were taken and analyzed by confocal microscopy (Zeiss, LSM700). For autophagy studies in cells, Hepa1c1c7 cells were transfected with GFP-LC3 plasmid and/or with 5–20 nM of siRNA for the indicated genes for 24–48 h. Cells were incubated in either complete media or serum free media for 24 h followed by 1 h in HBSS. Cells were treated with GW4064 overnight.

Fluorescent detection of lipophagy

Hepa1c1c7 cells were transfected with siRNAs and plasmids (GFP-LC3, CREB overexpression plasmid). After 36 h, cells were supplemented with 400 μm oleic acid (O3008, Sigma) for 6 h prior to incubation in HBSS for 3 h. Cells were fixed with 4% paraformaldehyde (#28908, Thermo scientific) and washed with PBS. A final concentration of 1 μg/ml of BODIPY 581/591 (D-3861, Life technologies) in 150 mM NaCl was used to stain for lipid for 10 min and then, cells were washed with PBS and counterstained with DAPI. For GW4064 treatment, Hepa1c1c7 cells were transfected with GFP-LC3, and 24 h later, cells were treated with GW4064 or DMSO for 6 h, incubated with HBSS for 3 h, and then, stained with BODIPY and counterstained with DAPI.

Biochemical localization study

Mice were fasted or fed overnight. Liver tissues (pooled from 3 WT or FXR-KO mice) were minced and then resuspended in hypotonic buffer and cells were lysed by homogenization. After centrifugation, the nuclear pellet and cytoplasmic supernatant were collected as previously described[25]. Cytoplasmic β-tubulin and nuclear lamin A were detected as controls for the quality of cellular fractionation.

Hepatocyte isolation and autophagy studies in cells

Primary hepatocytes were isolated by collagenase (0.8 mg/ml, Sigma-Aldrich Co.) perfusion through the portal vein of mice anesthetized with isoflurane as previously described[26]. Hepatocytes or Hepa1c1c7 cells were incubated with HBSS starvation media or with complete media and treated with vehicle, GW4064 (100 nM), rapamycin (100 nM), Torin (1 μM), chloroquine (50 μM), or bafilomycin A1 (100 nM) for the indicated times or siRNA (5–20 nM) for 48–72 h.

Liver ChIP and sequential re-ChIP

ChIP and re-CHIP assays were performed as previously described[24, 25]. Livers from WT or FXR-KO mice were minced and incubated in PBS containing 1% formaldehyde for 10 min, and glycine was added to a concentration of 125 mM. Minced liver was resuspended in hypotonic buffer and cells were lysed by homogenization. Nuclei were pelleted, resuspended and sonicated, and chromatin was IPed using 1–1.5 μg of antibody. For re-ChIP assays, CREB was IPed first and chromatin was eluted by adding 50 μl of 10 mM DTT at 37°C for 30 min. Then, the chromatin samples were diluted 20-fold with 20 mM Tris-HCl, pH 8.0, 150 mM NaCl, 2 mM EDTA, and 1% Triton X-100 and then re-IPed. The immunoprecipitates were extensively washed, chromatin was eluted, and the amounts of

genomic DNA were determined by semi-q PCR or q-PCR (primer sequences in Supplementary Table 6).

Tfeb-luc and Atg7-luc construction and luciferase assay

DNA fragments near the *Tfeb gene* (ch17:47907235-47908235) and the *Atg7 gene* (Chr6:114772715-114773373) that contained FXR peaks were amplified by PCR from mouse genomic DNA and cloned into the PGL3-SV40-Luc vector at the Kpn1/Nhe1 and SacI/BglII sites, respectively, and the cloning was confirmed by sequencing. A FXR mutant was constructed by mutation at the first zinc finger in the DNA binding domain. The values for luciferase activities were normalized to β-gal activities.

GST-pull down, CoIP, and q-RTPCR

Sequence encoding the FXR domains, AF1, DBD, or LBD, was amplified by PCR. The PCR product was inserted into the pGEX4T-1 vector at BamH1 and Xho1 sites. GST-FXR fusion proteins were expressed in *E. coli* BL21/DE3 and purified, CREB was synthesized in vitro by in vitro transcription and translation (TNT) (Promega, Inc), and GST-pull down assays were performed. For CoIP experiments, whole liver extracts from mice were prepared and the indicated proteins were immunoprecipitated and proteins in the immunoprecipitates were detected by IB. For q-RTPCR, total RNA was isolated, cDNA was synthesized, and q-RTPCR (primer sequences in Supplemental Table 7) was performed with an Applied Biosystems 7500 qPCR machine. The amount of mRNA was normalized to that of 36B4.

Gel mobility shift assay

Gel shift assays were done as previously described[24]. Double stranded oligonucleotides (31–32 mers) that contain the CREB binding site from *Atg7, Ulk1, and Tfeb* gene were labeled with [γ-^{32}P]ATP and incubated with purified CREB and FXR and with CRTC2 synthesized by TNT (Promega, Inc), in the presence of 100 ng poly dIdC and 20 μg BSA. For competition experiments, increasing amounts (1, 3, 15 ng) of unlabeled oligonucleotide competitors containing a CREB sequence (Supplementary Table 8) from *Atg7, Ulk1, Tfeb* (a consensus CREB site in the intron #1), *Tfeb* (a variant CREB site in the promoter), or *Pepck* as a positive control were incubated 5 min prior to adding the probe. Binding reactions were analyzed by electrophoresis in a low ionic TAE buffer with re-circulation of buffer.

Statistical analyses

Sample sizes were at least n=3 to allow statistical analysis and for image quantification 10–30 cells were counted. Values for Mean +/− SEM are presented. P values were generated using Student's t-test (* $p<0.05$, ** $p<0.01$).

ChIP-seq data analyses for FXR and CREB

We analyzed published ChIP-seq data for FXR[12, 13] and CREB[15, 19]. ChIP-seq reads were uniquely mapped to the mouse reference genome (mm9) by Bowtie with at most 2 mismatches. MACS was used to find ChIP-seq peaks with default parameters. Autophagy genes containing FXR or CREB binding peaks within 10 kb of the TSS were considered

potential FXR or CREB target genes. Genes were considered to have overlapping FXR-CREB binding peaks if the distance between the midpoints of the FXR and CREB binding peaks was less than 500 bp. To identify CREB binding motifs on 78 autophagy genes with overlapping sites, FIMO was used to search for two CREB known motifs within 500 bp of the midpoints between the centers of the overlapping FXR and CREB peaks using position weight matrices (PWM), MA0018.1 and MA0018.2, from the JASPAR database with $P < 0.001$.

Identification of transcription factor motifs within FXR binding peak regions

For the de novo motif analysis within the FXR peaks, the 36 motifs with the least motif score, 1.19, were identified using the Gibbs sampling method, with a maximum motif length set to 30 bp. 50,000 iterations for Markov chain Monte Carlo were used, the top 36 motifs were chosen for transcriptional factor identification. Motif similarity was analyzed using the on-line STAMP tools (http://www.benoslab.pitt.edu/stamp/).

Extended Data

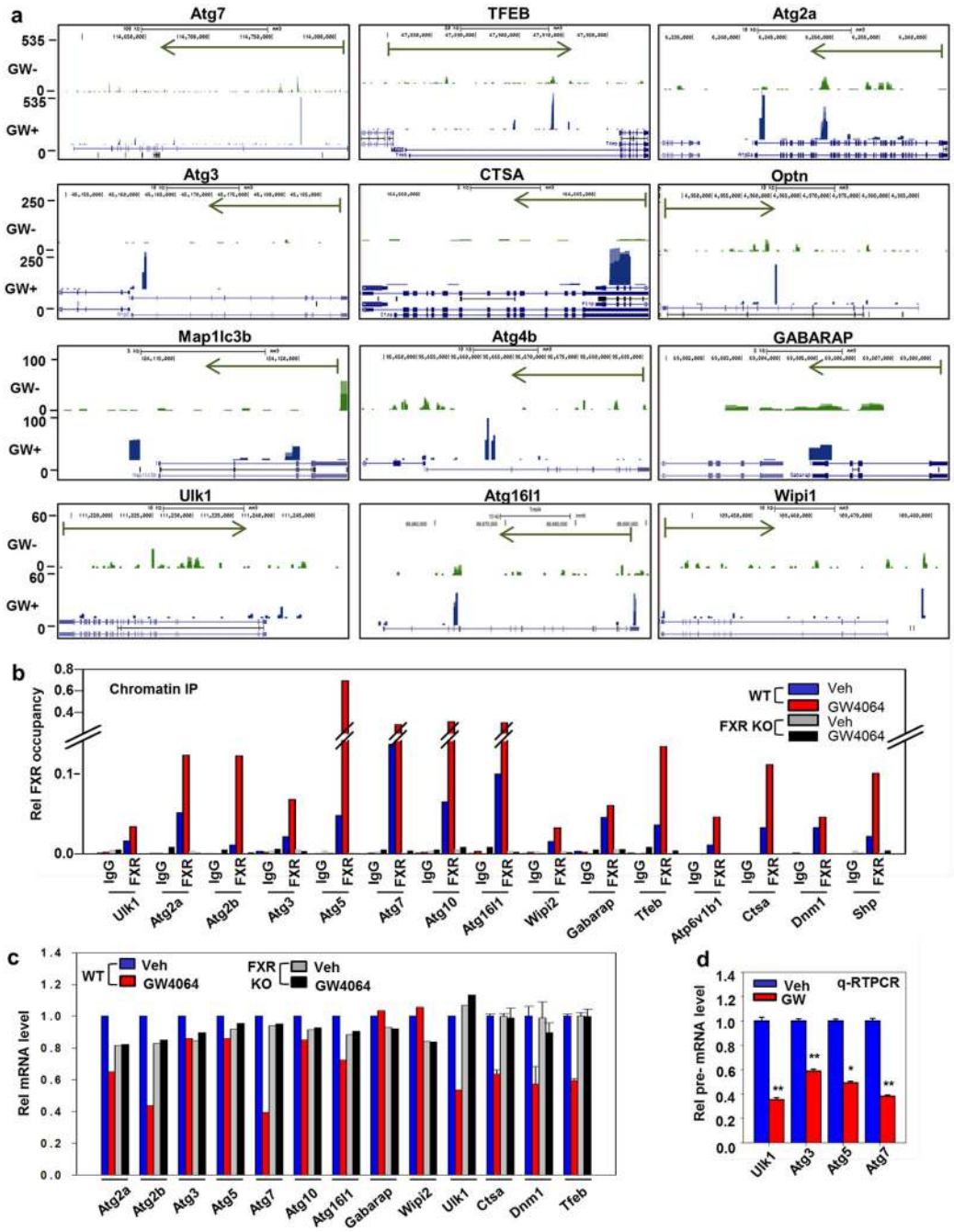

Extended Data Figure 1. Pharmacological activation of FXR increases its binding to hepatic autophagy genes and decreases their mRNA and pre-mRNA levels

(a) FXR binding peaks at selected autophagy-related genes. Figures were generated from mouse liver Chip-seq data using the USCD genome browser. Mice fed with normal chow diet (ND) and the GW- and GW+ tracks represent or mice treated with vehicle or GW4064 (GW+) for 1 h. The direction of gene transcription is indicated by the arrow and the beginning of the arrow indicates the position of the transcriptional starting site (TSS). **(b)**

WT or FXR-KO mice were fasted for 10 h and treated with GW4064 (30 mg/kg, i.p.) or vehicle for 6 h, and then liver tissues were harvested. Liver ChIP assays were performed to confirm occupancy of FXR at the indicated genes. **(c)** WT or FXR-KO mice were fasted for 10 h and treated with GW4064 (30 mg/kg, i.p.) or vehicle for 6 h. Livers were collected and mRNA levels of the indicated genes were determined by q-RTPCR. **(d)** WT mice were fasted for 10 h and treated with vehicle or GW4064 (30 mg/kg, i.p.) for 6 h. Livers were collected and pre-mRNA levels of the indicated genes were determined by q-RTPCR. For statistical analysis, n=3, SEM is shown, Student's t-test was used, and *p<0.05, **p<0.01.

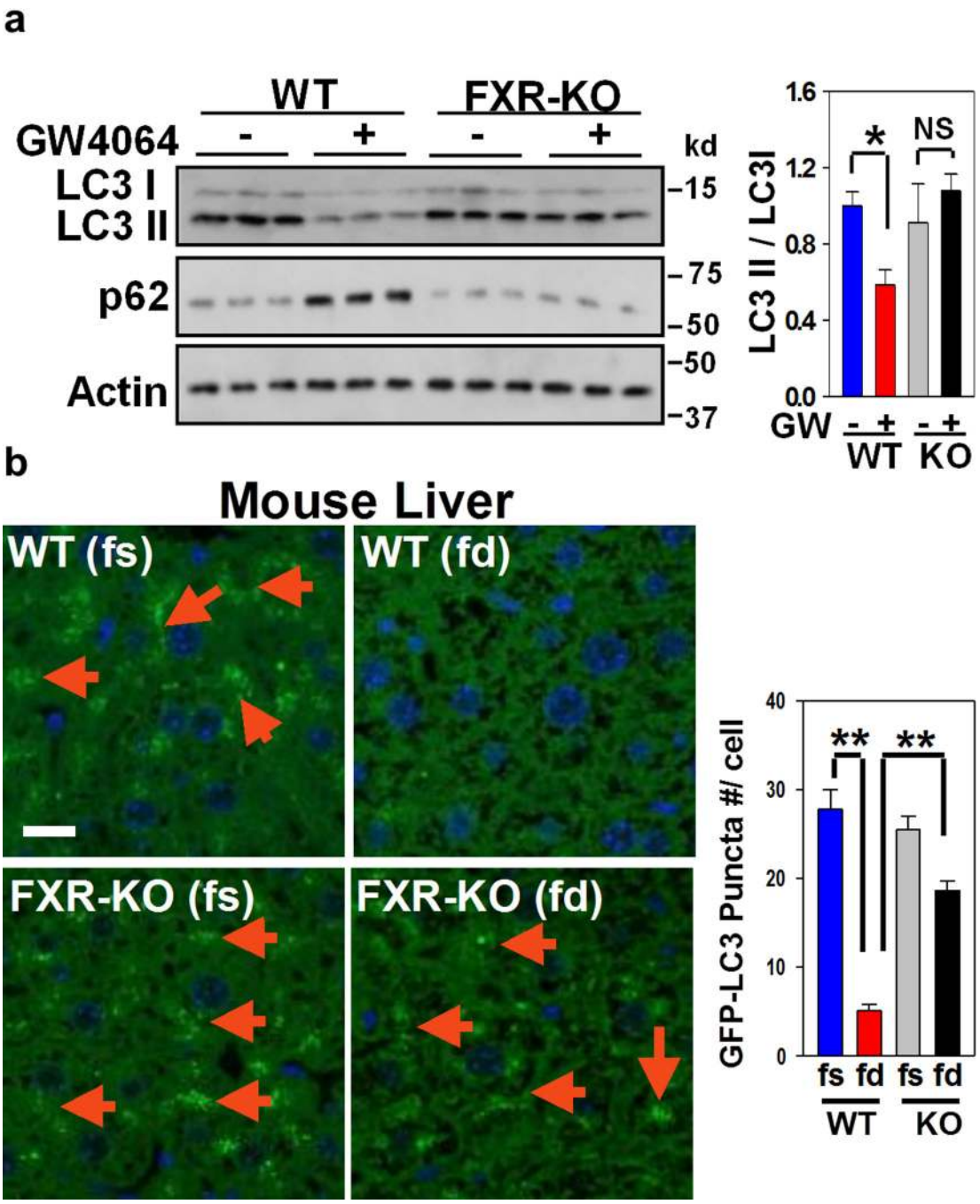

Extended Data Figure 2. Physiological and pharmacological activation of FXR signaling inhibits hepatic autophagy

(a) Primary hepatocytes were isolated from WT or FXR-KO mice and then treated with choloroquine (50 μM) for 30 min, and then, further treated with vehicle or GW4064 (100 nM) for 6 h, and IB was performed. LC3 and p62 levels in chloroquine-treated hepatocytes and quantitation. Representative images of GFP-LC3 puncta in livers of fasted or refed mice and its quantitation are shown (n=3). **(b)** Mice were tail vein injected with Ad-GFPLC3 and 1 week later, the mice were fasted overnight and livers were collected. The frozen or

paraffin-embedded liver sections were prepared for staining. Quantitation of GFP-LC3 in each experimental group is shown (n=15 hepatocytes). **(a,b)** For statistical analysis, SEM is shown, Student's t-test was used, and *p<0.05, **p<0.01.

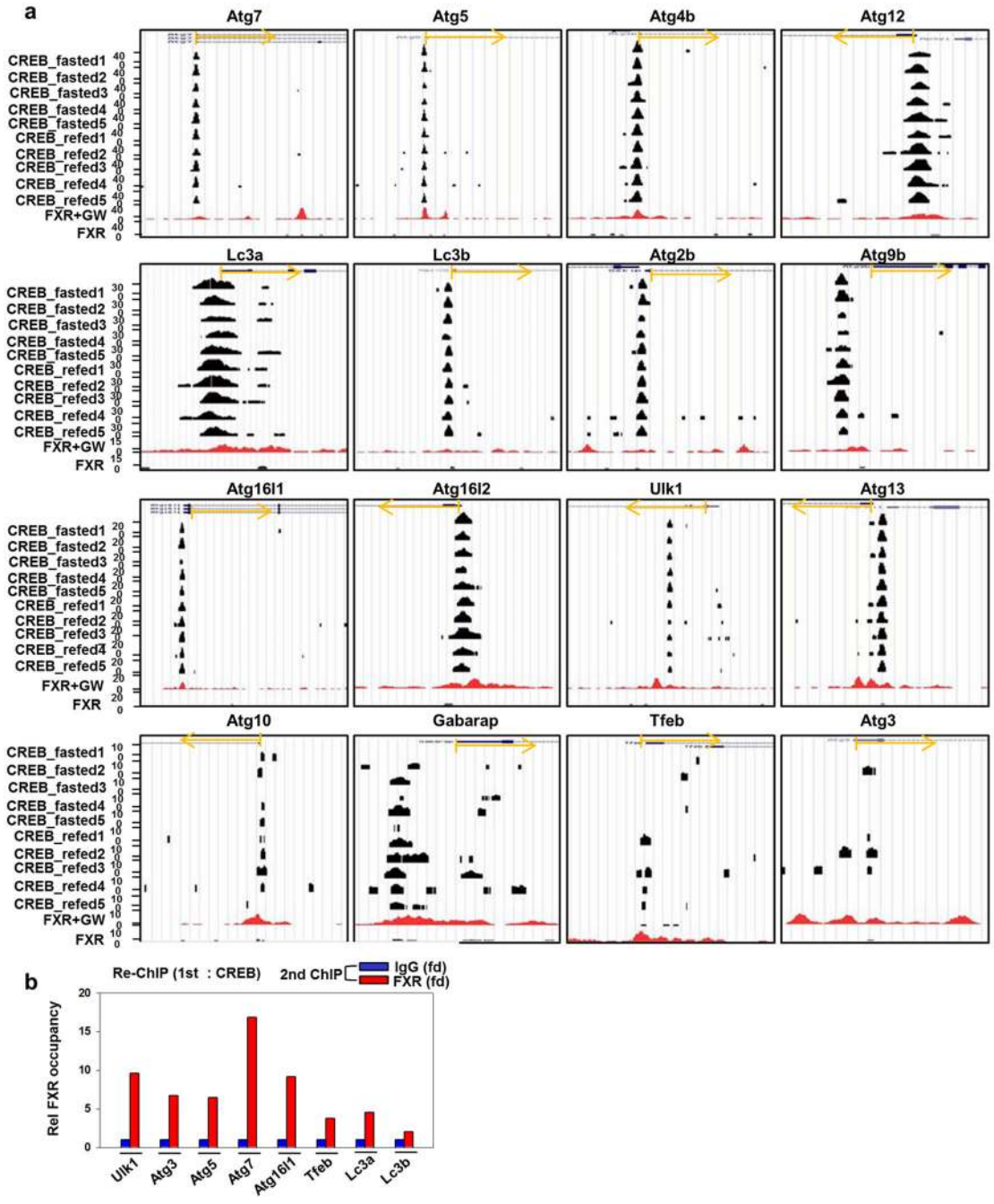

Extended Data Figure 3. Co-occupancy of FXR with CREB at selected autophagy-related genes in mouse liver

(a) Figures were generated from liver FXR ChIP-seq data for mice treated with GW4064 (FXR+GW) that are pooled from our group (Lee et. al, 2012) and from the G. Guo's group (Thomas et al., 2010), and for untreated mice (FXR) from our group. Binding peaks were

displayed using the USCD genome browser. CREB fasted or refed represents CREB1 ChIP-seq data from Everett et al., 2013 for WT mice fasted for 24 h or fasted for 24 h and then refed for 2 h, respectively. The direction of gene transcription is indicated by the arrow and the beginning of the arrow indicates TSS. **(b)** Mouse livers were harvested and pooled from two wild-type fed mice, and sequential re-ChIPs were performed first with CREB antibody then with FXR antibody or IgG. FXR occupancy at selected autophagy genes was checked by q-PCR.

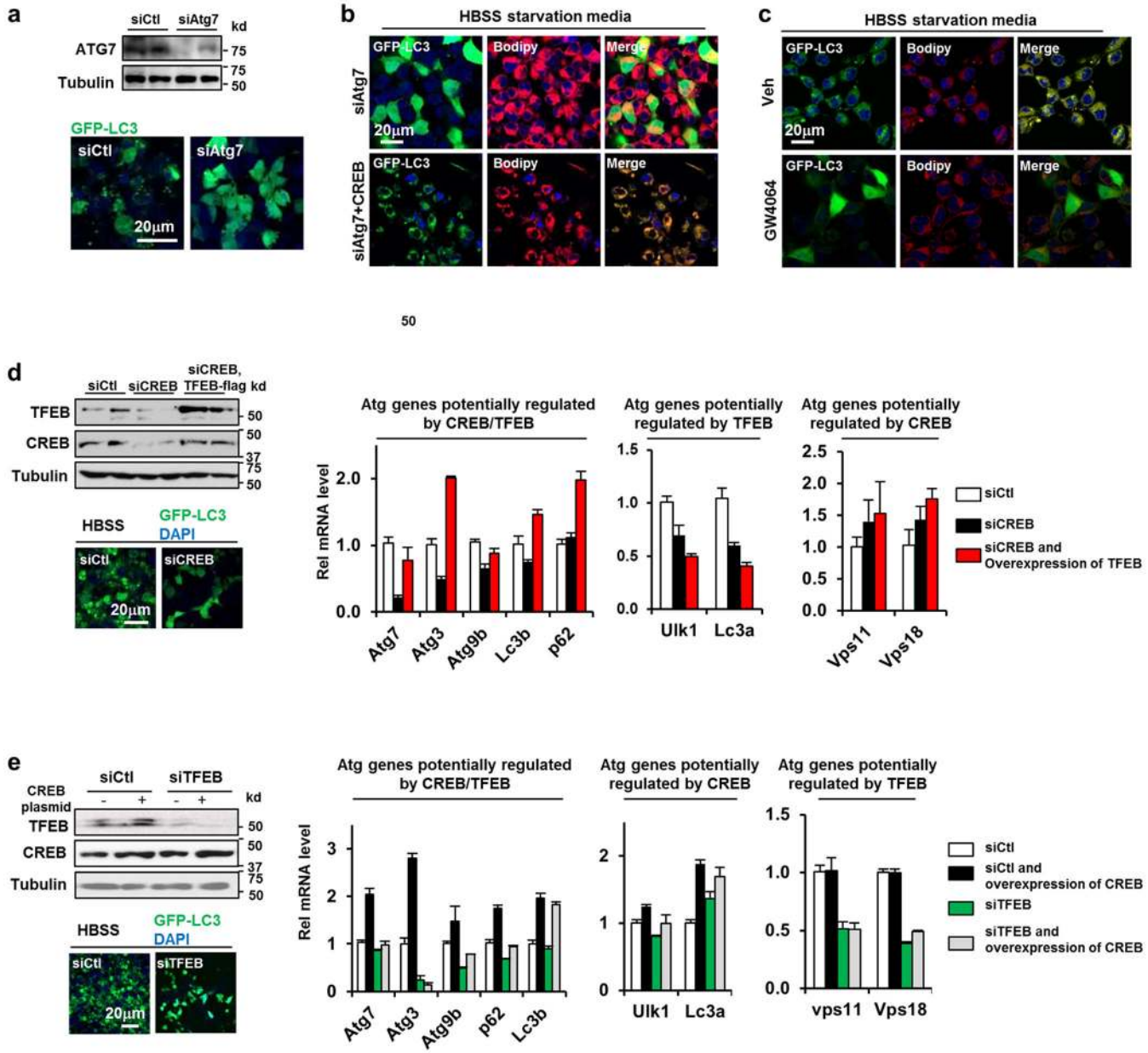

Extended Data Figure 4. Effects of downregulation of Atg7, CREB1, or TFEB on lipophagy and expression of autophagic and metabolic genes in Hepa1c1c7 cells

(a) Cells were incubated in HBSS for 3 h to mimic fasting, and Atg7 protein levels were determined by IB. Cells were transfected with the GFP-LC3 plasmid to monitor autophagic puncta in control and autophagy-deficient cells. Images were counterstained with DAPI. **(b)** Effects of downregulation of Atg7 and overexpression of CREB on lipophagy. **(c)** Effects of treatment with GW4064 on lipophagy in HBSS-incubated starved Hepa1c1c7 cells. **(d, e)** Hepa1c1c7 cells were transfected with siRNA or with an expression plasmid as indicated. **(d)** TFEB and CREB protein levels were measured by IB. GFP-LC3 fluorescence was used to monitor autophagy in fasted cells. mRNA levels of autophagy genes were measured by q-RTPCR. **(e)** TFEB and CREB protein levels were measured by IB. GFP-LC3 fluorescence was used to monitor autophagy in fasted cells. The mRNA levels of autophagy genes were measured by q-RTPCR. **(d,e)** For statistical analysis, n=3, SEM is shown.

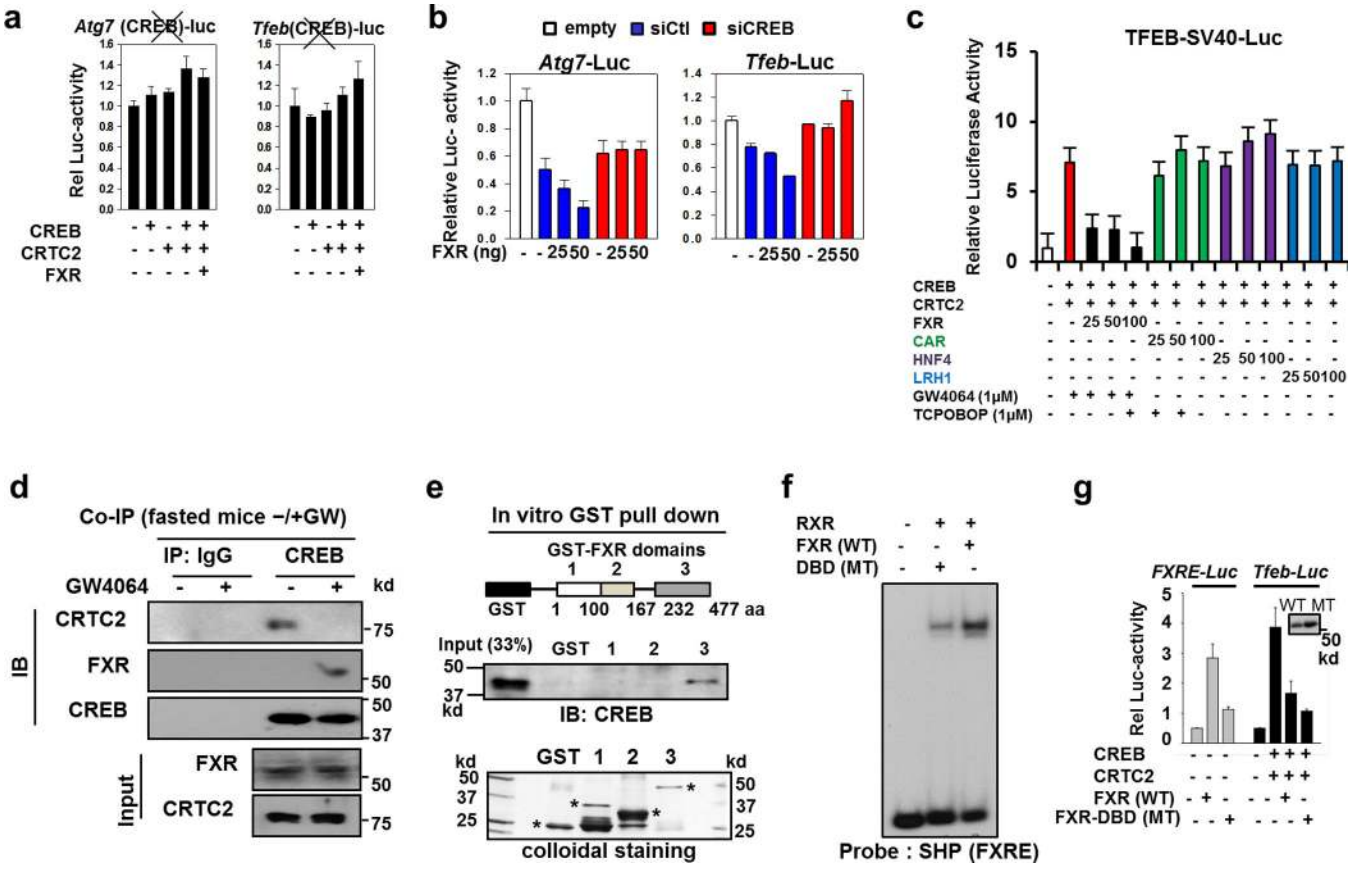

Extended Data Figure 5. FXR directly interacts with CREB and antagonizes transcriptional activity of CREB

(a) *Atg7 or Tfeb* DNA fragments that contained both FXR and CREB peaks sites were cloned and inserted into a luciferase vector. Neither expression of CREB and its coactivator CRTC2 nor expression of FXR increased luciferase activity after mutation of the CREB binding sites (indicated by the X). **(b)** Effects of downregulation of CREB in Hepa1c1c7 cells by siRNA on *Atg7 or Tfeb* luciferase reporter activity. The values for firefly luciferase activities were normalized by β-galactosidase activities. For statistical analysis, n=3, SEM is shown. **(c)** Hepa1c1c7 cells were transfected with the *Tfeb-Luc* reporter, with CREB and CRTC2 expression plasmids, and with increasing amounts of expression plasmids for FXR,

CAR, HNF4 and LRH1. Cells were treated with GW4064 and TCPOBOP for 3 h to activate FXR and CAR, respectively. The values for firefly luciferase activities were normalized by β-galactosidase activities. **(d)** CoIP assays: Mice were fasted for 10 h, and then treated with GW4064 or vehicle for 6 h. Livers were pooled (n=3), CREB was IPed from whole cell extracts, and the levels of CRTC2, FXR and CREB levels in the immunoprecipitates were determined by IB. **(e)** GST-pull down assays: At the top, different fragments of GST-FXR were purified as GST fusion proteins as indicated and analyzed by colloidal staining after SDS-PAGE at the bottom. Binding of CREB to the GST proteins was detected by IB (middle panel). **(f, g)** Effects of DBD mutation on repression of autophagy genes. **(f)** In vitro gel shift assays were performed utilizing partially purified RXR and FXR proteins (WT or DBD mutant by mutation at the first zinc finger) synthesized by in vitro transcription and translation (TNT, Promega, Inc). **(g)** Luciferase reporter assays: Effects of an FXR DBD mutant (MT) on *Tfeb-luc* activity.

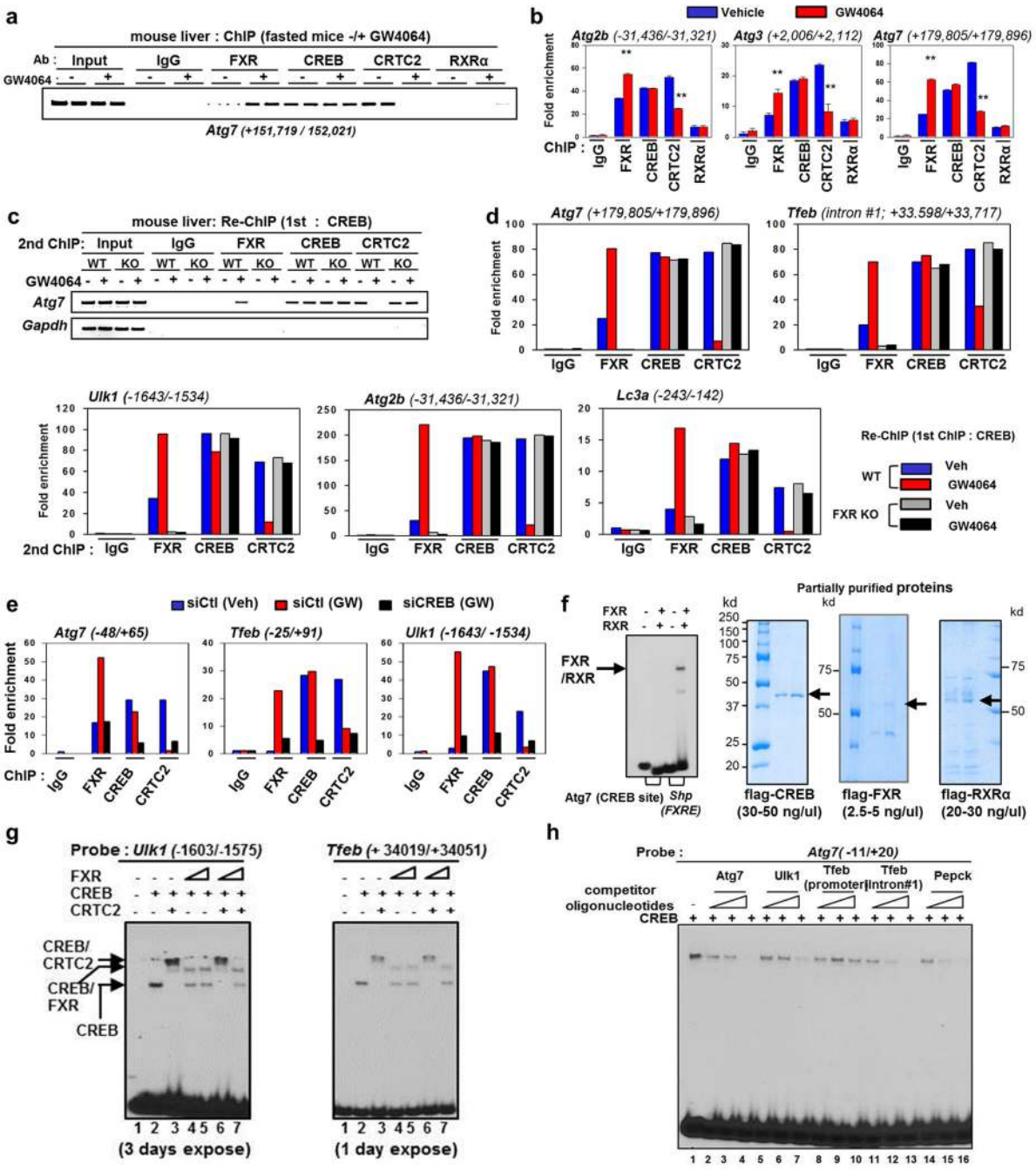

Extended Data Figure 6. Effects of GW4064 treatment on occupancy of FXR, CRTC2, and RXR at CREB-bound autophagy genes in mouse liver

(a, b) Liver ChIP: Mice (n=3) were fasted for 10 h, and then treated with GW4064 or vehicle for 6 h. Livers were collected, and ChIP assays were performed. Occupancy of FXR, CREB, CRTC2, and RXR at the *Atg2b, Atg3, and Atg7* genes was detected by **(a)** semi-quantitative analysis or **(b)** q-PCR analysis. **(c, d)** Liver re-ChIP: WT or FXR-KO mice were fasted for 10 h and were treated with GW4064 or vehicle for 6 h, livers were pooled from three mice, and re-ChIP assays were performed to detect FXR, CREB, and CRTC2

occupancy using semi-quantitative PCR analysis **(c)** or q-PCR **(d)** at the indicated positions of the genes. **(e)** Hepa1c1c7 cells were transfected with siCREB or siCtl for 36 h, and then treated with GW4064 or vehicle for 6 h. Cells were harvested, and ChIP assays were performed. Occupancy of FXR, CREB, and CRTC2 at the *Atg7, Tfeb, and Ulk1* genes was detected by q-PCR. **(f–h)** gel shift assays: **(f)** FXR, RXR, and CREB were partially purified (**f**, right 3 panels) and FXR/RXR was incubated with a radiolabeled *Atg7 or Shp* fragment and **(g)** FXR, CREB, and TNT-synthesized CRTC2 was incubated with radiolabeled *Ulk1 or Tfeb* fragments containing a CREB motif. **(h)** Competition gel shift assay: Increasing amounts (1, 3, 15 ng) of oligonucleotide competitors (31–32 mer) containing CREB sites from the indicated genes were incubated with CREB for 5 min before adding the probe. The CREB sequence from the *Pepck* gene serves as a positive control. Similar results were observed from 2 independent experiments. **(b)** For statistical analysis, n=3, SEM is shown, Student's t-test was used, and **p<0.01.

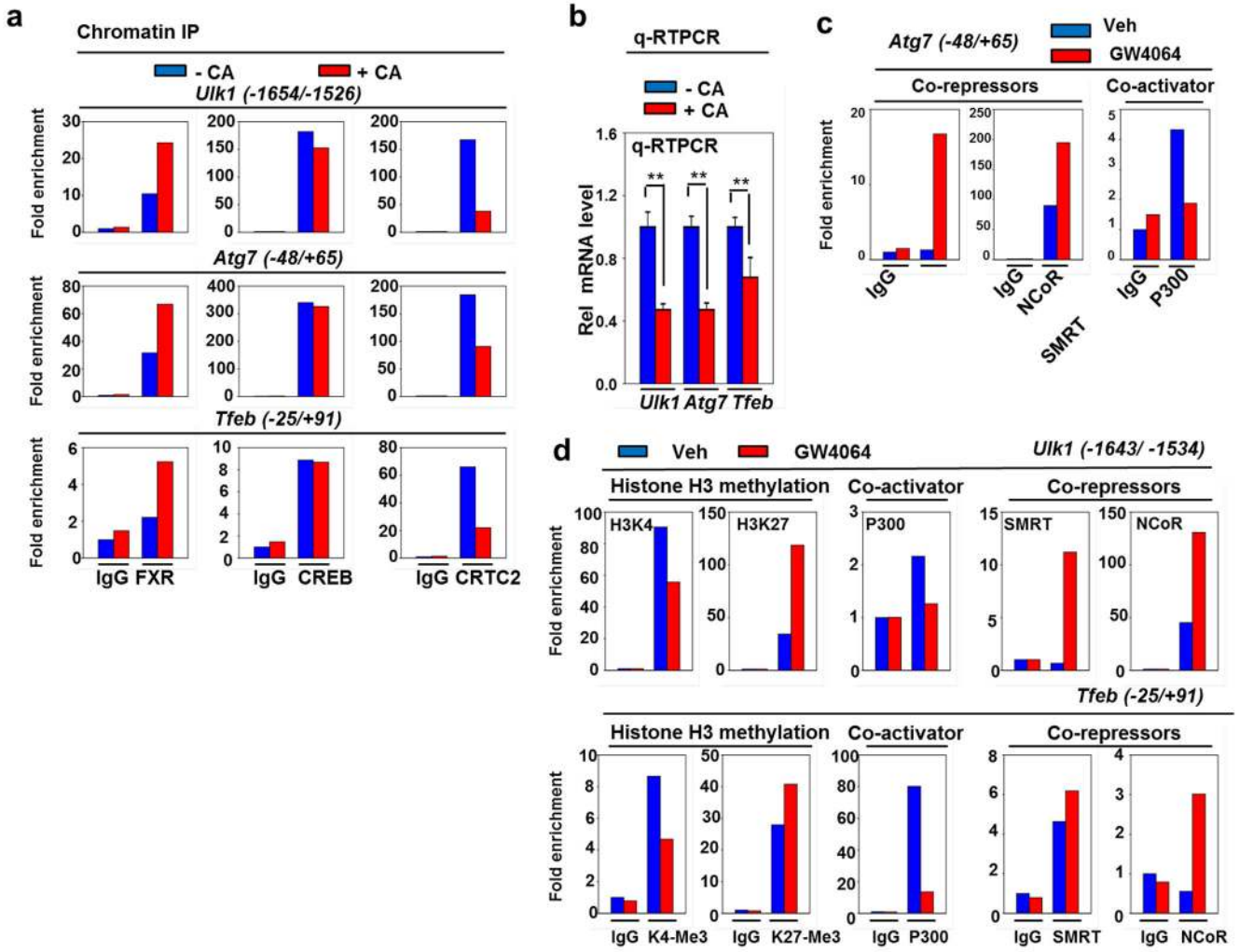

Extended Data Figure 7. Effect of cholic acid (CA) chow on occupancy of FXR, CREB, and CRTC2 at selected autophagy genes

Mice fasted for 10 h were refed with CA chow or normal chow for 6 h, then livers were collected. **(a)** FXR, CREB, CRTC2 occupancies at *Ulk1, Atg7*, and *Tfeb* genes at the indicated gene positions were determined by q-PCR of ChIP assays. **(b)** mRNA levels of *Ulk1, Atg7*, and *Tfeb* genes were measured by q-RTPCR. **(c, d) Effects of GW4064 treatment on occupancy of transcriptional coregulators and histone H3 methylation at *Atg7, Tfeb, and Ulk1* genes in mouse liver.** ChIP: Mice fasted for 10 h were treated with GW4064 or vehicle for 6 h, livers were collected (pooled from n=2 mice), and ChIP assays were performed. Occupancy of P300, SMRT, and NCoR, and levels of H3K4-Me3 (gene-activation histone mark) and H3K27-Me3 (gene-repression histone mark) at the *Atg7, Ulk1 and Tfeb* promoter regions were detected by q-PCR analysis.

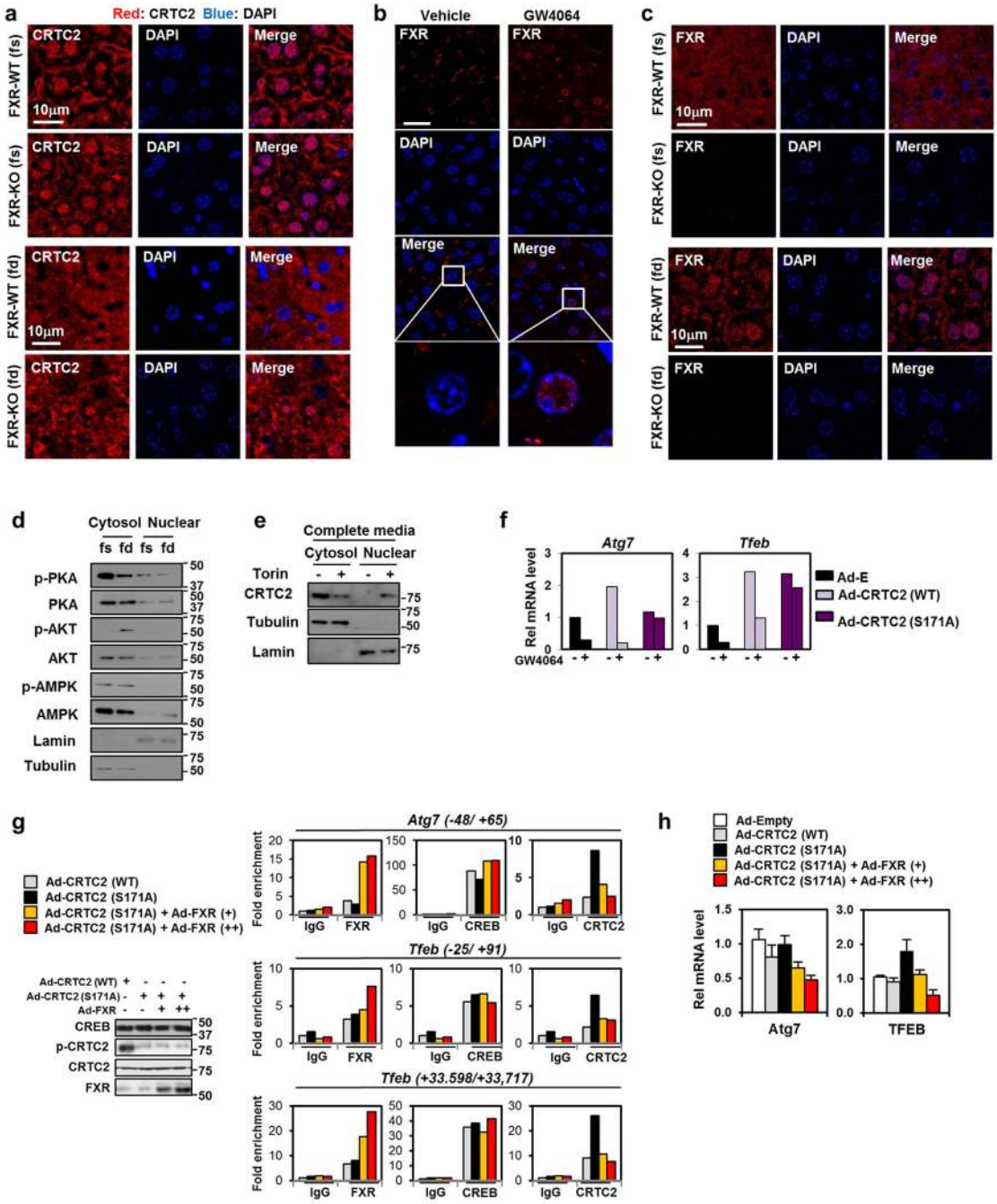

Extended Data Figure 8. Effects of GW4064 treatment or feeding/fasting on nuclear localization of FXR, CREB, and CRTC2, and phosphorylated PKA, PKB, and AMPK levels

(a) Effects of fasting and feeding on localization of CRTC2 in WT and FXR-KO mice. CRTC2 staining (red), DAPI (blue), and merged images are shown. **(b)** Effects of GW4064 on nuclear localization of FXR in WT mouse liver. **(c)** Effects of fasting or feeding on localization of FXR in WT and FXR-KO mice. FXR staining (red), DAPI (blue), and merged images are shown. **(d)** Nuclear and cytoplasmic extracts were isolated from fasting or fed WT mice. Lamin and tubulin were measured by IB to monitor the quality of nuclear

and cytosol isolation, respectively. Levels of total and phosphorylated PKA, AKT, AMPK were measured by IB. **(e)** Hepa1c1c7 cells were treated with Torin (1 mM) for 1 h and the levels of endogenous CRTC2 in the nucleus and cytosol were determined by IB. **(f)** Effects of phosphorylation at S171of CRTC2 on inhibition of *Atg7 and Tfeb* genes by GW4064 treatment for 6 h and then mimic fasting in HBSS for 1 h in Hepa1c1c7 cells. **(g, h)** Hepa1c1c7 cells were cultured in completed media and infected with Ad-CRTC2 (WT), Ad-CRTC2(S171A), or Ad-FXR as indicated. Expression of indicated proteins were determined by IB (left) and the occupancy of FXR, CREB, and CRTC2 were determined by ChIP-qPCR. Consistent results were observed from 2 independent experiments. Expression of *Atg7 and Tfeb* genes were detected by q-RTPCR (SEM, n=6).

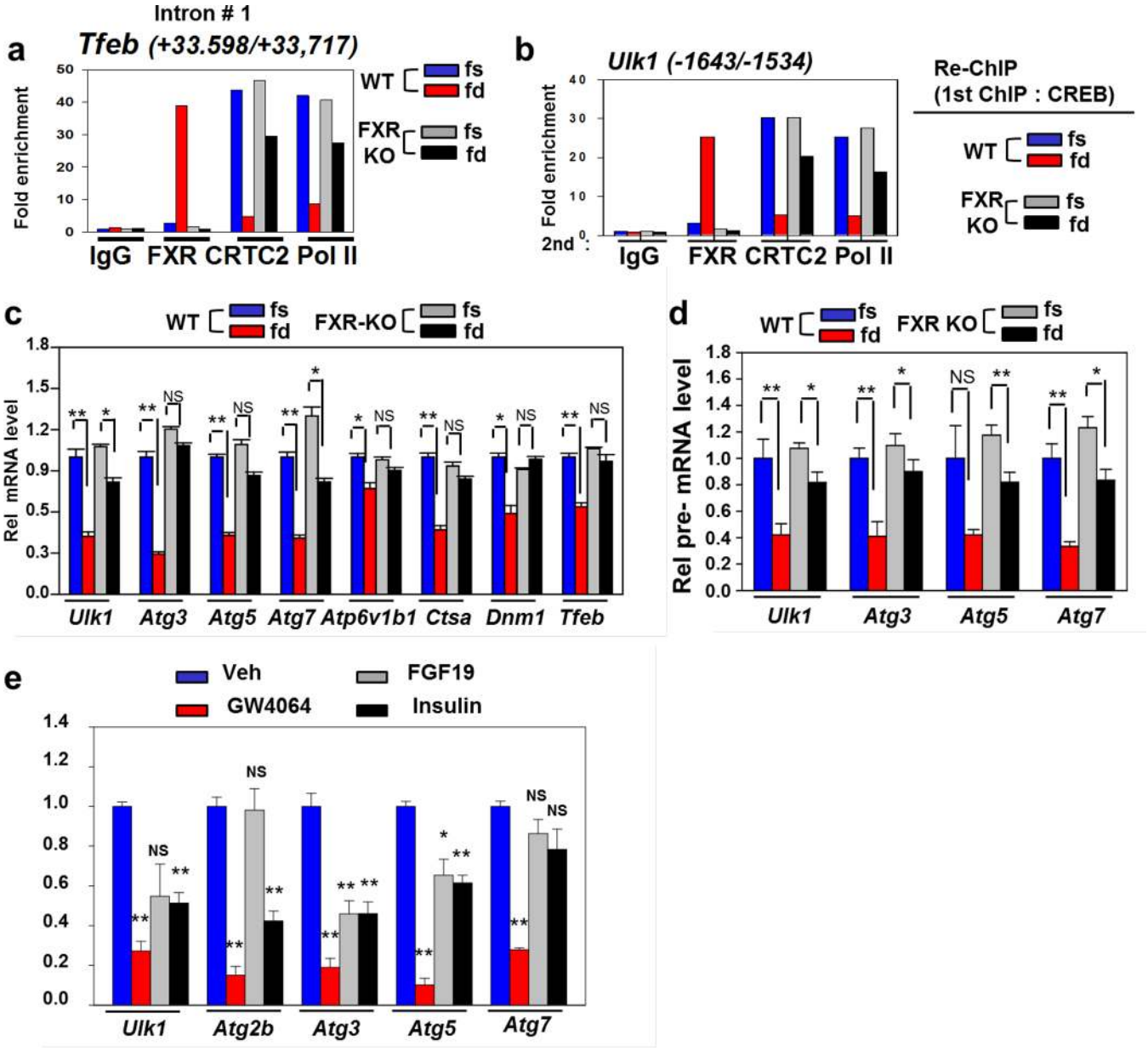

Extended Data Figure 9. Effects of fasting/feeding on occupancy of FXR, CRTC2, and RNA Pol II at the autophagy-related genes and mRNA and pre-mRNA levels of autophagy genes

(a) Re-ChIP in WT and FXR-KO mice (pooled from 3 mice). Occupancy of FXR, CREB, and CRTC2 at the *Tfeb* gene intron # 1 region containing a consensus CREB. **(b)** Re-ChIP: Effects of GW4064 treatment or feeding on occupancy of FXR, CREB, and CRTC2 at the *Ulk1* gene in WT and FXR-KO mice. **(c, d)**, WT or FXR-KO mice were fasted for 10 h and then fed or fasted for 6 h. **(c)** mRNA and **(d)** pre-mRNA levels of autophagy genes were measured by q-RTPCR. **(e)** Primary hepatocytes were treated with GW4064, FGF19, or Insulin, and autophagy gene expression was measured by q-RTPCR. **(c–e)** For statistical analysis, n=3, SEM is shown, Student's t-test was used, and *p<0.05, **p<0.01.

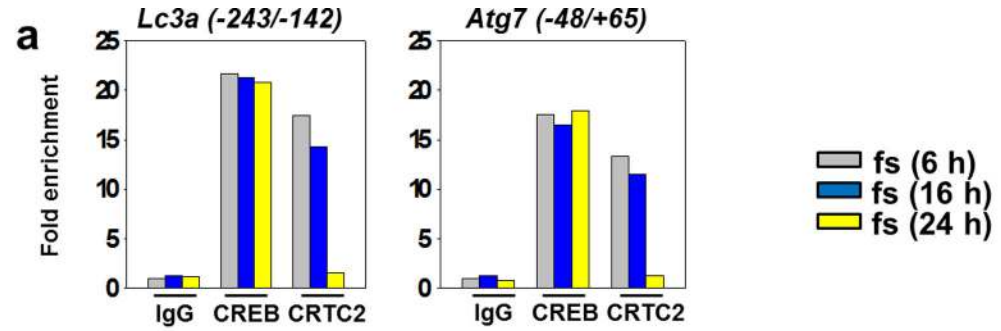

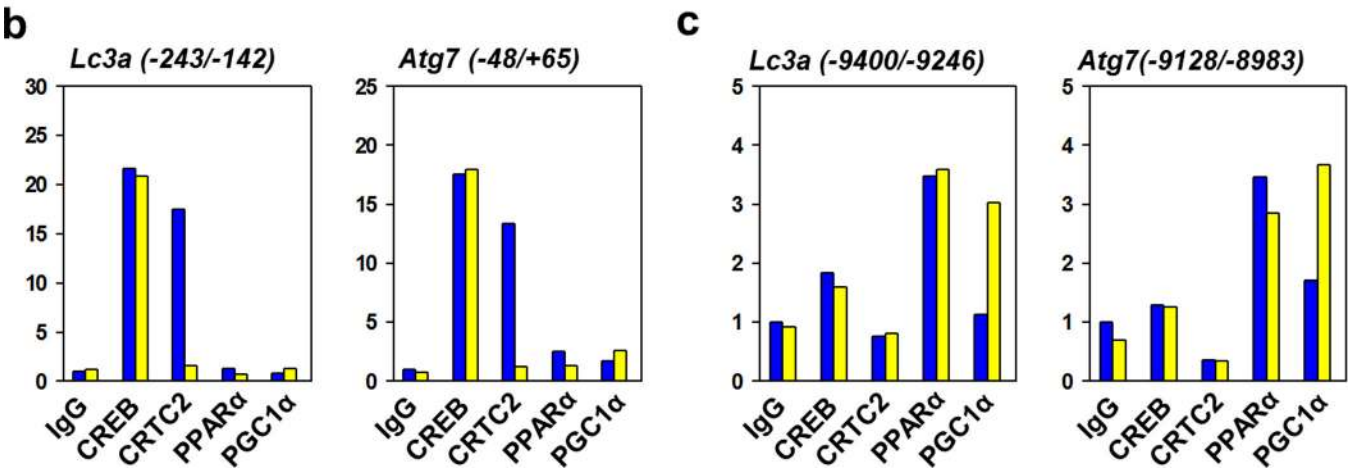

Extended Data Figure 10. Fasting time-dependent occupancy of CREB/CRTC2 and PPARα/PGC-1α at different regions of *Atg7 and Lc3a* genes

(a) Mice were fasted for 6 h, 16h, or 24 h and ChIP assays were performed. Occupancy of CREB/CRTC2 at the *Lc3a* and *Atg7* genes. **(b, c)**, Mice were fasted for 16 h or 24 h and ChIP assays were performed. Occupancy of CREB/CRTC2 and PPARα/PGC1α at different FXR binding peak regions of the *Lc3a* and *Atg7 genes* were detected. A relatively short fasting, 6 or 16 h, appears to be important for CREB/CRTC2 occupancy in the promoter regions of these genes, while a longer term 24 h fasting is important for PPARα/PGC1α occupancy at distal regions of these genes.

Supplementary Material

Refer to Web version on PubMed Central for supplementary material.

Acknowledgments

We thank Daniel Ryerson and David Tkac for constructing the pGEX4T-FXR clones. We thank Marc Montminy for providing Ad-CRTC2 and Ad-CRTC2-S171A, Seung-Hoi Koo for CREB and CRTC2 plasmids, Gokhan Hotamisligil for Ad-GFP-LC3, and Rosa Puertollano for flag-TFEB plasmid. This study was supported by grants from the National Institutes of Health (DK62777 and DK95842) to JKK.

References

1. Levine B, Klionsky DJ. Development by self-digestion: molecular mechanisms and biological functions of autophagy. Dev. Cell. 2004; 6:463–477. [PubMed: 15068787]
2. Rabinowitz JD, White E. Autophagy and metabolism. Science. 2010; 330:1344–1348. [PubMed: 21127245]
3. Sachdeva UM, Thompson CB. Diurnal rhythms of autophagy: implications for cell biology and human disease. Autophagy. 2008; 4:581–589. [PubMed: 18437053]
4. Mizushima N. Physiological functions of autophagy. Curr. Top. Microbiol. Immunol. 2009; 335:71–84. [PubMed: 19802560]
5. Kim J, Kundu M, Viollet B, Guan KL. AMPK and mTOR regulate autophagy through direct phosphorylation of Ulk1. Nat. Cell Biol. 2011; 13:132–141. [PubMed: 21258367]
6. Egan DF, et al. Phosphorylation of ULK1 (hATG1) by AMP-activated protein kinase connects energy sensing to mitophagy. Science. 2011; 331:456–461. [PubMed: 21205641]
7. He C, Klionsky DJ. Regulation mechanisms and signaling pathways of autophagy. Annu. Rev. Genet. 2009; 43:67–93. [PubMed: 19653858]
8. Calkin AC, Tontonoz P. Transcriptional integration of metabolism by the nuclear sterol-activated receptors LXR and FXR. Nat. Rev. Mol. Cell Biol. 2012; 13:213–224. [PubMed: 22414897]
9. Thomas C, Pellicciari R, Pruzanski M, Auwerx J, Schoonjans K. Targeting bile-acid signalling for metabolic diseases. Nat Rev Drug Discov. 2008; 7:678–693. [PubMed: 18670431]
10. Koo SH, et al. The CREB coactivator TORC2 is a key regulator of fasting glucose metabolism. Nature. 2005; 437:1109–1111. [PubMed: 16148943]
11. Wang Y, Vera L, Fischer WH, Montminy M. The CREB coactivator CRTC2 links hepatic ER stress and fasting gluconeogenesis. Nature. 2009; 460:534–537. [PubMed: 19543265]
12. Lee J, et al. Genomic analysis of hepatic Farnesoid X Receptor (FXR) binding sites reveals altered binding in obesity and direct gene repression by FXR. Hepatol. 2012; 56:108–117.
13. Thomas AM, et al. Genome-wide tissue-specific farnesoid X receptor binding in mouse liver and intestine. Hepatology. 2010; 51:1410–1419. [PubMed: 20091679]
14. Everett LJ, et al. Integrative genomic analysis of CREB defines a critical role for transcription factor networks in mediating the fed/fasted switch in liver. BMC Genomics. 2013; 14 337-2164-14-337.
15. Zhang X, et al. Genome-wide analysis of cAMP-response element binding protein occupancy, phosphorylation, and target gene activation in human tissues. Proc. Natl. Acad. Sci. U. S. A. 2005; 102:4459–4464. [PubMed: 15753290]
16. Singh R, et al. Autophagy regulates lipid metabolism. Nature. 2009; 458:1131–1135. [PubMed: 19339967]
17. Mizushima N, Yoshimori T, Levine B. Methods in mammalian autophagy research. Cell. 2010; 140:313–326. [PubMed: 20144757]
18. Inagaki T, et al. Fibroblast growth factor 15 functions as an enterohepatic signal to regulate bile acid homeostasis. Cell Metab. 2005; 2:217–225. [PubMed: 16213224]
19. Luo Q, et al. Mechanism of CREB recognition and coactivation by the CREB-regulated transcriptional coactivator CRTC2. Proc. Natl. Acad. Sci. U. S. A. 2012; 109:20865–20870. [PubMed: 23213254]
20. Settembre C, et al. TFEB links autophagy to lysosomal biogenesis. Science. 2011; 332:1429–1433. [PubMed: 21617040]
21. Settembre C, et al. TFEB controls cellular lipid metabolism through a starvation-induced autoregulatory loop. Nat. Cell Biol. 2013; 15:647–658. [PubMed: 23604321]

22. Yang L, Li P, Fu S, Calay ES, Hotamisligil GS. Defective hepatic autophagy in obesity promotes ER stress and causes insulin resistance. Cell. Metab. 2010; 11:467–478. [PubMed: 20519119]

23. Levine B, Kroemer G. Autophagy in the pathogenesis of disease. Cell. 2008; 132:27–42. [PubMed: 18191218]

24. Kemper JK, et al. FXR acetylation is normally dynamically regulated by p300 and SIRT1 but constitutively elevated in metabolic disease states. Cell Metabolism. 2009; 10:392–404. [PubMed: 19883617]

25. Seok S, et al. Bile acid signal-induced phosphorylation of small heterodimer partner by protein kinase Czeta is critical for epigenomic regulation of liver metabolic genes. J. Biol. Chem. 2013; 288:23252–23263. [PubMed: 23824184]

26. Fu T, et al. Aberrantly elevated microRNA-34a in obesity attenuates hepatic responses to FGF19 by targeting a membrane coreceptor beta-Klotho. Proc. Natl. Acad. Sci. U. S. A. 2012; 109:16137–16142. [PubMed: 22988100]

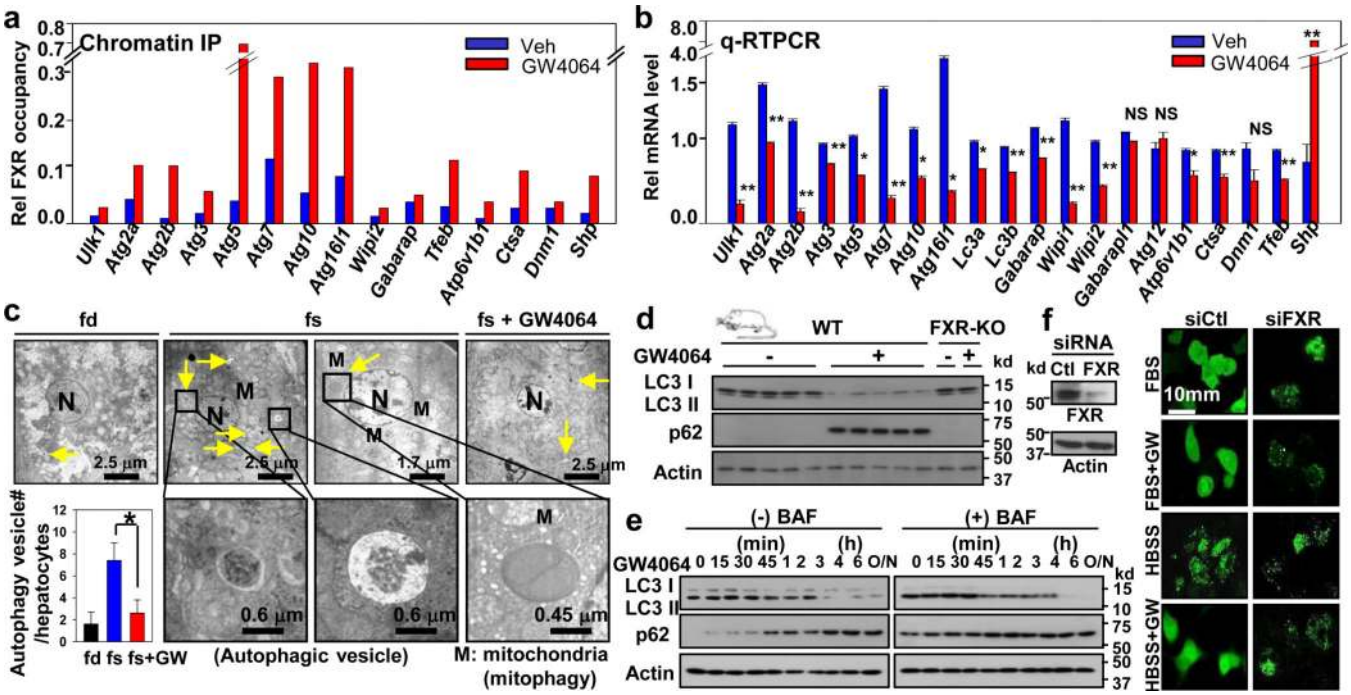

Fig. 1. Pharmacological activation of FXR transcriptionally inhibits hepatic autophagy

FXR occupancy **(a)** and mRNA levels **(b)** in mice treated with GW4064 for 6 h after 10 h fasting, (n=3). **(c)** Electron microscopy of liver sections. Arrows indicate autophagosomes and mitophagy, (n=10 hepatocytes). **(d)** Hepatic LC3 and p62 levels in WT or FXR-KO mice. **(e)** Effects of bafilomycin A1 (BAF) and/or GW4064 on LC3 and p62 levels in hepatocytes. **(f)** GFP-LC3 fluorescence in Hepa1c1c7 cells, HBSS (starvation media) and GW (GW4064). **(b–c)** SEM is shown, statistical analysis by Student's t-test, *p<0.05,**p<0.01

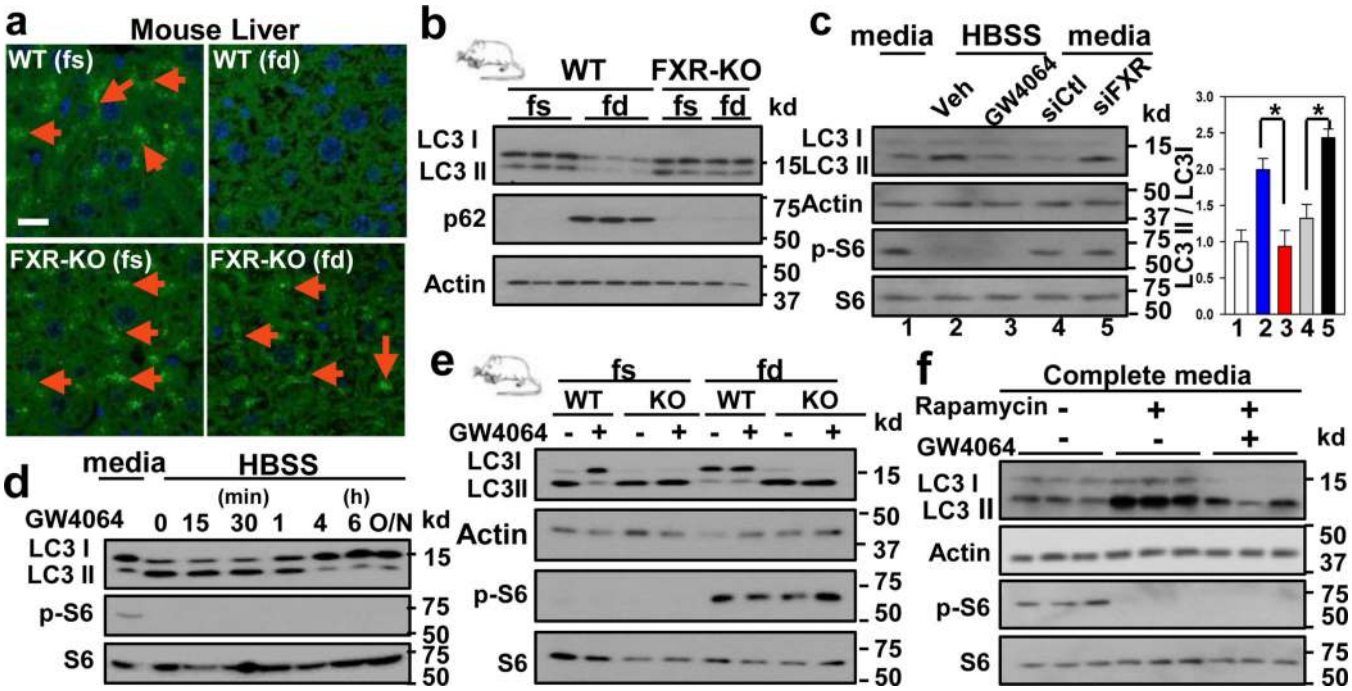

Fig. 2. FXR is a physiological repressor of hepatic autophagy in the fed state

(a) Representative images from 5 total of GFP-LC3 puncta in livers of fasted or refed mice tail-vein injected with Ad-GFPLC3. Quantification is in Extended Data Fig. 2b. **(b)** Effects of feeding/fasting on liver LC3 and p62 levels. **(c–e)** Effects of GW4064 or downregulation of FXR on LC3 and p-S6 levels in hepatocytes **(c,d)** or mice (pooled from 3 mice) **(e)**. **(f)** Effects of rapamycin and/or GW4064 on p-S6 and S6 levels in hepatocytes. **(c)** For statistical analysis, n=3, SEM is shown, Student's t-test was used, and *p<0.05.

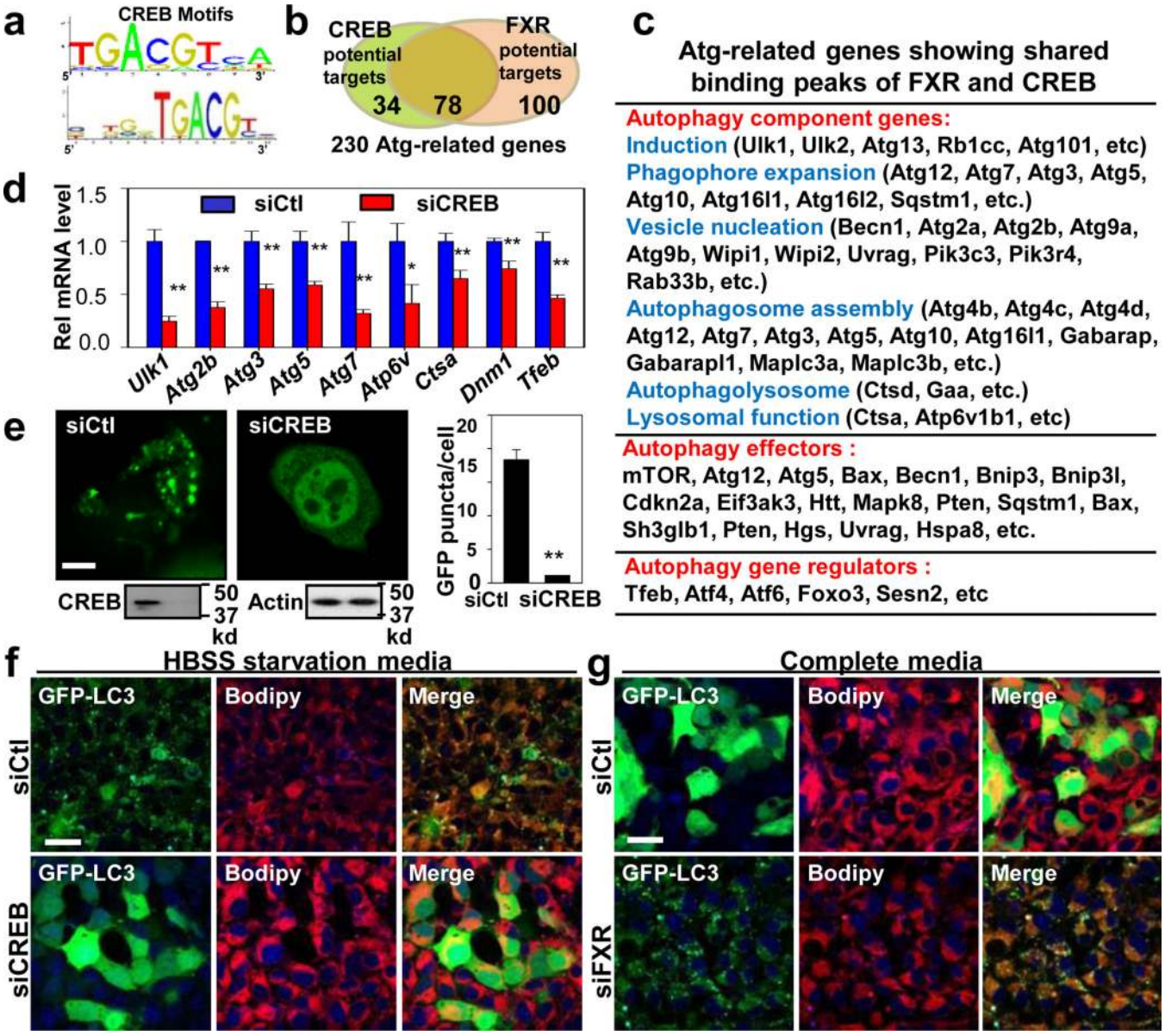

Fig. 3. CREB is a new transcriptional activator of autophagy, and CREB and FXR oppositely regulate lipophagy

(a) CREB binding motif logos **(b)** Venn diagram showing autophagy genes that contain the FXR and CREB peaks within 10 kb from the TSS. **(c)** A list of autophagy genes showing overlapping peaks of FXR and CREB. **(d, e)** Effects of downregulation of CREB on autophagy gene expression **(d)** and GFP-LC3 puncta **(e)** in Hepa1c1c7 cells incubated with HBSS. **(f, g)** Effects of downregulation of CREB **(f)** or FXR **(g)** on lipophagy in Hepa1c1c7 cells. **(d,e)** For statistical analysis, n=3, SEM is shown, Student's t-test was used (*p<0.05, **p<0.01).

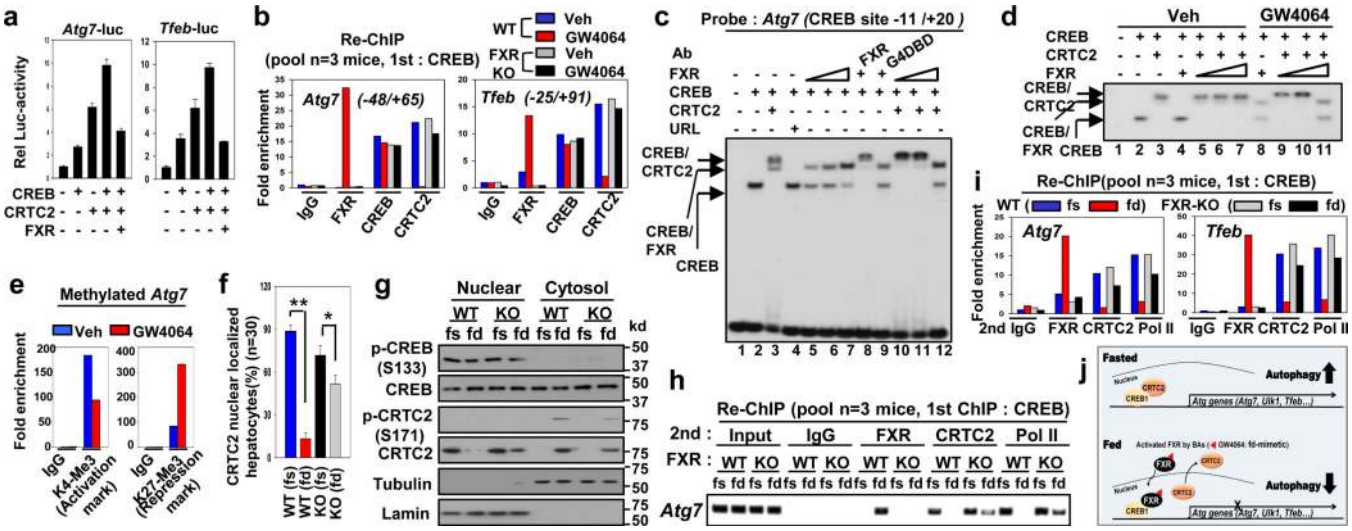

Fig. 4. FXR trans-represses autophagy genes by disrupting the CREB/CRTC2 complex

(a) *Atg7-luc and Tfeb-luc* activities in Hepa1c1c7 cells (n=3, SEM). **(b)** Re-ChIP: Protein occupancy in WT and FXR-KO mice. **(c, d)** Gel shift assay: An *Atg7* probe contains overlapping CREB/FXR peaks. **(e)** ChIP: Effects of GW4064 on histone methylations at the *Atg7* promoter. **(f)** Effects of feeding/fasting on nuclear localization of CRTC2 in liver, quantitation (n=30 hepatocytes, SEM is shown, statistical analysis by Student's t-test,*, $p<0.05$, **$p<0.01$). **(g)** p-CREB, p-CRTC2 and CRTC2 levels in nuclear and cytoplasmic extracts. **(h, i)** Re-ChIP: Effects of feeding/fasting on protein occupancy in WT and FXR-KO mice. **(j)** Model: During fasting, autophagy-related genes are induced by CREB/CRTC2, and after feeding, activation of FXR signaling contributes to disruption of the CREB/CRTC2 complex and trans-repression of these genes.